Surface waters of the NW Iberian margin: upwelling on the shelf *versus* outwelling of upwelled waters from the Rías Baixas

X.A Álvarez–Salgado[1], J. Gago[1], B.M. Míguez[2], M. Gilcoto[1, 2] and F.F. Pérez[1]

1 CSIC, Instituto de Investigacións Mariñas, Eduardo Cabello 6, 36208–Vigo, Spain

2 Facultade de Ciencias do Mar, Universidade de Vigo, Lagoas–Marcosende, 36200–Vigo, Spain

Running head: *Outwelling versus Upwelling in NW Spain*

Version: 4 September 2000

Key words: upwelling, downwelling, outwelling, box model, Spanish rías

Abstract

A set of hydrographic surveys were carried out in the Ría of Vigo (NW Spain) at 2–4 d intervals during four 2–3 wk periods in 1997, covering contrasting seasons. Residual exchange fluxes with the adjacent shelf were estimated with a 2D, non–steady–state, salinity–temperature weighted box model. Exchange fluxes consist of a steady–state term (dependent on the variability of continental runoff) and a non–steady–state term (dependent on the time changes of density gradients in the embayment). More than 95% of the short–time–scale variability of the exchange fluxes in the middle and outer ría can be explained by the non–steady–state term that, in turns, is correlated (r^2 >75%) with the offshore Ekman transport. Conversely, 96% of the variability of exchange fluxes in the inner ría rely on the steady–state term. The outer and middle ría are under the direct influence of coastal upwelling, which enhances the positive residual circulation pattern by an order of magnitude: from 10^2 to 10^3 m^3 s^{-1}. On the contrary, downwelling provokes a reversal of the circulation in the outer ría. The position of the downwelling front along the embayment depends on the relative importance of Ekman transport (Q_X, m^3 s^{-1} km^{-1}) and continental runoff (R, m^3 s^{-1}). When Q_X/R > 7±2 the reversal of the circulation affects the middle ría. Our results are representative for the 'Rías Baixas', four large coastal indentations in NW Spain. During the upwelling season (spring & summer), 60% of shelf surface waters off the 'Rías Baixas' consist of fresh Eastern North Atlantic Central Water (ENACW) upwelled *in situ*. The remaining 40% consists of upwelled ENACW that previously enters the rías and it is subsequently outwelled after thermohaline modification. During the downwelling season (autumn & winter), 40% of the warm and salty oceanic subtropical surface water, which piled on the shelf by the predominant southerly winds, enters the rías.

Glossary of Selected Terms

$\overline{\beta}/\overline{\alpha}$	Average coefficient of haline contraction/thermal expansion at the boundary of the study box between 2 consecutive surveys
$\overline{E}$	Average evaporation in the study box between 2 consecutive surveys
ε_D, ε_S, ε_T	Error of $\Delta S/\Delta t$ (or $\Delta T/\Delta t$), $\overline{S_B}$ (or $\overline{S_S}$), $\overline{T_B}$ (or $\overline{T_S}$)
$\varepsilon_H, \varepsilon_R, \varepsilon_Q, \varepsilon_{QZ}, \varepsilon_{MZ}$	Error of $\overline{H}$, $\overline{R}$, $\overline{Q_B}$ (or $\overline{Q_S}$), $\overline{Q_Z}$, $\overline{M_Z}$
$\overline{H}$	Average air–sea heat exchange flux between 2 consecutive surveys
$\overline{M_Z}$	Average vertical mixing in the study box between 2 consecutive surveys
$\overline{P}$	Average precipitation in the study box between 2 consecutive surveys
$\overline{Q_B}$, $\overline{Q_S}$	Average bottom and surface horizontal convective fluxes at the boundary of the study box between 2 consecutive surveys
$-\overline{Q_X}$	Average offshore Ekman transport between 2 consecutive surveys
$\overline{Q_Z}$	Average vertical advection in the study box between 2 consecutive surveys
$\overline{R}$, $\overline{R \cdot T_R}$	Average river water and heat fluxes between 2 consecutive surveys
$\Delta S/\Delta t$, $\Delta T/\Delta t$	Changes in the salt and heat content of the study box between 2 consecutive surveys
$\overline{S_B}$, $\overline{S_S}$	Average bottom and surface salinity at the boundary of the study box between 2 consecutive surveys
$\overline{T_B}$, $\overline{T_S}$	Average bottom and surface temperature at the boundary of the study box between 2 consecutive surveys
V	Volume of the study box
$\lvert V \rvert$, V_y	Wind speed and north component of wind speed recorded at the Cape Finisterre Meteorological Observatory
$\overline{w}$	Weighting factor of the relative contribution of salinity and temperature to the density gradient

Introduction

Enhanced shelf–edge exchange is the reason behind the intensified primary production, recycling and export of organic matter in ocean margins (Wollast, 1998). Primary production rates in coastal upwelling areas (average 420 g C m^{-2} y^{-1}) is almost twice as in the global coastal zone (250 g C m^{-2} y^{-1}; Schlesinger, 1997). This high fertility and the enhanced horizontal fluxes cause that organic matter export from upwelling regions is 10 to 100 times higher than in other coastal systems (Barber & Smith, 1981; Walsh, 1991). Coastal upwelling occurs at the four major eastern boundary current regions of the World Ocean: Canary, California, Benguela and Perú/Humboldt (Bakun & Nelson, 1991).

The western coast of the Iberian Peninsula is the northern boundary of the NW Africa coastal upwelling system that associates with the Canary Current. At these latitudes (37°–43°N) shelf winds follow a seasonal pattern connected to the large–scale climatology of the NE Atlantic. Upwelling–favourable northerly winds predominate from March–April to September–October whilst downwelling–favourable southerly winds prevail the rest of the year (Wooster et al., 1976; McClain et al, 1986; Bakun & Nelson, 1991). The cold and nutrient–rich Eastern North Atlantic Central Water (ENACW) is promoted to the shelf during upwelling events (Fraga 1981; Fiúza, 1983). Warm and salty surface waters of subtropical origin pile on the shelf during the downwelling period (Haynes & Barton, 1990; 1991). However, the analysis of a 1987–96 time series of daily offshore Ekman transport values at 43°N revealed that this seasonal pattern explains <20% of the observed variability. More than 70% of the total variability concentrates at frequencies <30 days (Nogueira et al., 1997; Nogueira, 1998). Consequently, the wind–induced fertility and export of materials in NW Spain have to be evaluated through process–orientated studies at the short–time–scale. Álvarez–Salgado et al. (1993) observed that the frequency of upwelling episodes at 43°N was 14±4 days and designed an intensive sampling programme visiting the study site every 3–4 days. This sampling frequency allowed them to adequately follow the response of the water column to periodic upwelling episodes. Their strategy has been recurrently applied to study the hydrodynamics (Rosón et al., 1997), chemistry (e.g. Álvarez–Salgado et al., 1996) and biology (e.g. Gómez–Fermín et al., 1996) of the system during the productive upwelling season.

Wind–driven upwelling causes a complex circulation pattern in upwelling areas, which involves the combination of 2–layer along–shore and 2–layer off–shore fluxes. A poleward–flowing bottom current compensates the equatorward–flowing surface current. Concomitantly, Ekman pumping provokes the offshore deflection of the surface flux and the compensating inshore & upward displacement of the bottom flux (Barber & Smith, 1981). The northern boundary of the western Iberian Peninsula (42°–43°N) is occupied by the 'Rías Baixas', four large coastal indentations under the direct influence of shelf wind–stress (Fig. 1a). The along–shore component of the flux can be neglected in these embayments (Rosón et al., 1997). In the present work, the short–time–scale 2D circulation pattern of the Ría of Vigo will be examined under four contrasting meteorological and hydrographic conditions: spring, summer, autumn and winter. We approach the problem with a simplified version of the 2D, non–steady–state, salinity–temperature weighted box model successfully applied by Rosón et al. (1997) to the adjacent Ría of Arousa. Previous 2D box model studies of water circulation in the Ría of Vigo (Prego et al., 1990; Prego & Fraga, 1992) used a steady–state approach, which is inappropriate to model the short–time–scale circulation pattern. In addition, these models were based just on salinity changes. Therefore, they fail specially during the upwelling season, when density gradients are mainly caused by temperature.

Our key aim is to establish the relative importance of **1**) upwelling of ENACW on the shelf and **2**) outwelling of upwelled ENACW from the Rías Baixas in the composition of shelf surface waters. This topic has important implications for the biogeochemistry of shelf waters off the Rías Baixas (López–Jamar et al., 1992; Tenore et al., 1995; Álvarez–Salgado et al., 1997), the study site of the EU project 'Ocean Margin Exchange II' (Fig. 1a).

Material and methods

Sampling programme and measured variables

The Ría of Vigo was visited aboard *R/V* 'Mytilus' during four contrasting periods in 1997: 7–23 April, 1–18 July, 15 September–2 October and 1–12 December. Full–depth continuous conductivity and temperature profiles were recorded with a calibrated CTD SBE–25 at four selected stations along the main axe of the embayment (stns 1, 2, 3 and 5), and one additional site at the shallow northern entrance of the Ría of Vigo (stn 4; Fig. 1b). Salinity was calculated from the CTD–conductivity record with the equation of UNESCO (1985). The accuracy of CTD salinity and temperature was ±0.005 and ±0.005°C, respectively. This programme was repeated every 2–4 days during each period. A total of 6 surveys were performed in April, July and September–October, and 4 surveys in December.

In parallel to the hydrographic programme, key meteorological data such as shelf (*V*x, *V*y) and local (*W*x, *W*y) wind components, precipitation rates (*P*), humidity (*h*), cloudiness (*N*) and air temperature (T_A) were collected during the sampling periods. Shelf winds were recorded at the Cape Finisterre Meteorological Observatory (Fig. 1a), a representative site for winds blowing off the 'Rías Baixas' (Álvarez–Salgado et al., 1993). Local winds were taken from the Meteorological Observatory at the base laboratory in Bouzas (Fig. 1b). Daily precipitation (mm d^{-1}), humidity (%) and cloudiness (in oktas) were taken from the Meteorological Observatory at Vigo Airport and corrected taking into account its altitude above the sea level.

Variables calculated from collected data

Daily values of the offshore Ekman transport ($-Q_X$, $m^3\ s^{-1}\ km^{-1}$), were calculated according to Wooster et al. (1976):

$$-Q_X = -\frac{\rho_{air} \cdot C_D \cdot |V| \cdot V_y}{\rho_{sw} \cdot f} \qquad (1)$$

Where ρ_{air} is the density of air, 1.22 kg·m^{-3} at 15°C. C_D is an empirical drag coefficient (dimensionless), 1.3·10^{-3} according to Hidy (1972). f is the Coriolis parameter, 9.946·10^{-5} s^{-1} at 43° latitude. ρ_{SW} is the density of seawater, ~1025 kg·m^{-3}. $|V|$ and V_y are the average daily wind speed and the north component of wind speed recorded at the Cape Finisterre Meteorological Observatory.

Continental runoff to the Ría of Vigo per unit area (R/A, in l m^{-2} d^{-1}) was estimated according to Ríos et al. (1992) empirical equation, using precipitation (P) in the drainage basin:

$$\frac{R}{A} = \frac{1-k}{k-k^{365+1}} \cdot \sum_{n=1}^{365} P(n) \cdot k^n \qquad (2)$$

This equation considers the influence of daily precipitation during the year before the study day. k is the retention constant, with a value of 0.75 for the 586 km^2 drainage basin of the Ría of Vigo (Ríos et al., 1992).

Evaporation rates (E, mm d^{-1}) were calculated with Otto's (1975) empirical equation, based on local wind velocity (W, m s^{-1}) and vapour pressure at the sea surface (e_S, in mbar) and 2 m above the sea surface (e_Z):

$$E = (0.26 + 0.077 \cdot W) \cdot (e_S - e_Z)$$

$$e_Z = e_{T_A} \cdot \frac{h}{100} \qquad (3)$$

$$e_S = e_{T_S} \cdot (1 - 0.000537 \cdot S_S)$$

Where S_S (in pss) and T_S (in °C) are surface salinity and temperaure. e_{T_A} and e_{T_S} (in mm Hg) are the distilled water vapour pressure at T_A and T_S, which can be calculated for temperatures between 5°C and 22 °C with:

$$e_T = 4.589 + 0.330 \cdot T + 0.011 \cdot T^2 + 1.53 \cdot 10^{-4} \cdot T^3 + 3.74 \cdot 10^{-6} \cdot T^4 \qquad (4)$$

Heat exchange with the atmosphere (*H*) was evaluated considering the balance of the following terms: irradiation, conduction, back radiation, reflection and heat lost by evaporation. Irradiation (*I*, cal cm^{-2} d^{-1}) was calculated with the equation developed by Rosón et al. (1997) for 42°N:

$$I = \left[3.191 + 1.115 \cdot sin^2 \left(\pi \cdot \frac{355 - J}{365} \right) \right] \cdot \left(50.417 - 4.474 \cdot N \right) \quad (5)$$

J is Julian day, from 1 (1 January) to 365 (31 December). Conduction (*C*, in cal cm^{-2} d^{-1}) was obtained following Otto's (1975) empirical equation that depends on the temperature gradient between the sea surface (T_S, in °C) and the atmosphere (T_A), and on local wind speed (*W*, in m s^{-1}).

$$C = 24.88 \cdot \left(0.38 + 0.114 \cdot W \right) \cdot \left(T_S - T_A \right) \quad (6)$$

The back radiation term (*B*, cal cm^{-2} d^{-1}) was estimated with the equation (Laevastu, 1963):

$$B = \left(297 - 1.87 \cdot T_S - 0.96 \cdot h \right) \cdot \left(1 - 0.1 \cdot N \right) \quad (7)$$

Heat lost by reflection is assumed to represent 6% of irradiation at our latitudes (Otto, 1975). Finally, evaporation also implies a loss of energy that can be calculated by multiplying the rate of evaporation *E* (in mm d^{-1}) times 58.7 cal cm^{-2} mm^{-1}.

The 2D box model

A simplified version of the 2D, non–steady–state, salinity–temperature weighted box model successfully applied by Rosón et al. (1997) to the adjacent Ría of Arousa is presented in this work. This box model is able to estimate the average water fluxes (horizontal and vertical advection, vertical mixing) which

produce the salinity and temperature changes observed in the Ría of Vigo between 2 consecutive surveys, separated 2–4 days.

Three boundaries are considered, which delimit the inner and outer part of the Ría of Vigo (Fig 1b). The inner limit separates the ría from San Simón Bay, the estuary of the river Oitabén–Verdugo. The outer limit separates the ría from the continental shelf off the 'Rías Baixas'. The middle limit separates the small (0.5 km^3), shallow (average 15m) inner box exposed to San Simón Bay fluxes from the large (2.26 km^3) and deeper (average 27m) outer box exposed to exchange with the adjacent shelf waters.

The three boundaries are divided in two layers (surface, bottom), flowing in opposite directions. The limit between the surface and bottom layer (level of no–horizontal motion) is the gravity centre of the boundary, *i.e*. the depth where the actual density coincides with the average density of the boundary (Rosón et al., 1997). The average salinity and temperature of the surface and bottom layer of every boundary and box are obtained by numeric integration of the calibrated CTD profiles considering the geometric characteristics of each boundary and box. For any of the three boundaries, the average surface layer water, salt and heat fluxes between two consecutive surveys —from t_1 to t_2— are:

$$\overline{Q_S} = \frac{\int_{t_1}^{t_2} Q_S(t) \cdot dt}{t_2 - t_1} \tag{8}$$

$$\overline{Q_S \cdot S_S} = \frac{\int_{t_1}^{t_2} Q_S(t) \cdot S_S(t) \cdot dt}{t_2 - t_1} \tag{9}$$

$$\overline{Q_S \cdot T_S} = \frac{\int_{t_1}^{t_2} Q_S(t) \cdot T_S(t) \cdot dt}{t_2 - t_1} \tag{10}$$

Where $Q_S(t)$, $S_S(t)$ and $T_S(t)$ are the evolution of surface water, salt and heat fluxes from t_1 to t_2, respectively. Average bottom water ($\overline{Q_B}$) salt ($\overline{Q_B \cdot S_B}$) & heat ($\overline{Q_B \cdot T_B}$) fluxes, and fresh water ($\overline{R}$) &

heat ($\overline{R \cdot T_R}$) fluxes from t_1 to t_2 can be calculated accordingly from $Q_B(t)$, $S_B(t)$, $T_B(t)$, $R(t)$ and $T_R(t)$. The net freshwater input to each box is the balance of precipitation (*P*), evaporation (*E*) and continental runoff (*R*).

A simple system of three linear equations —conservation of water (11), salt (12) and heat (13)— can be written for the volume of the ría delimited within each of the three boundaries. This is, San Simón Bay for the case of boundary 1, San Simón Bay + the inner ría for the case of boundary 3 and San Simón Bay + the inner ría + the outer ría for the case of boundary 4.

$$\overline{Q}_S = \overline{Q}_B + \overline{R} \tag{11}$$

$$V \cdot \frac{\Delta S}{\Delta t} = \overline{Q_B \cdot S_B} - \overline{Q_S \cdot S_S} \tag{12}$$

$$V \cdot \frac{\Delta T}{\Delta t} = \overline{Q_B \cdot T_B} - \overline{Q_S \cdot T_S} + \overline{R \cdot T_R} + \overline{H} \tag{13}$$

Additional simplifications are necessary to solve the system of equations:

$$\overline{Q_B \cdot S_B} - \overline{Q_S \cdot S_S} \sim \overline{Q}_B \cdot \overline{S}_B - \overline{Q}_S \cdot \overline{S}_S \tag{14}$$

$$\overline{Q_B \cdot T_B} - \overline{Q_S \cdot T_S} + \overline{R \cdot T_R} \sim \overline{Q}_B \cdot \overline{T}_B - \overline{Q}_S \cdot \overline{T}_S + \overline{R} \cdot \overline{T}_R \tag{15}$$

These simplifications are based on the extreme variability of water fluxes (Q_S, Q_B and R) compared with salinity and temperature changes (S_S, T_S, S_B, T_B and T_R) between two consecutive surveys in the study system (Rosón et al., 1997).

Two sets of horizontal convective fluxes can be obtained, from the equations of water (11) and salt (12, 14) conservation, $(\overline{Q}_S)_S$:

$$(\overline{Q}_S)_S = \frac{\overline{R} \cdot \overline{S}_B + V \cdot \frac{\Delta S}{\Delta t}}{\overline{S}_B - \overline{S}_S} \tag{16}$$

And the equations of water (11) and heat (13, 15) conservation, $(\overline{Q}_S)_T$:

$$(\overline{Q}_S)_T = \frac{\overline{R} \cdot (\overline{T}_B - \overline{T}_R) - \overline{H} + V \cdot \frac{\Delta T}{\Delta t}}{\overline{T}_B - \overline{T}_S} \tag{17}$$

A salinity–temperature weighted horizontal flux, $\overline{Q}_S$, can be obtained as follows:

$$\overline{Q}_S = (\overline{Q}_S)_S \cdot (1 - \overline{w}) + (\overline{Q}_S)_T \cdot \overline{w} \tag{18}$$

The dimensionless weighting factor, $\overline{w}$, is calculated as:

$$\overline{w} = \frac{(\overline{T}_B - \overline{T}_S)^2}{(\overline{T}_B - \overline{T}_S)^2 + (\overline{S}_B - \overline{S}_S)^2 \cdot (\overline{\beta}/\overline{\alpha})^2} \tag{19}$$

$\overline{w}$ weights the contribution of salinity and temperature to the density gradient at the boundary of the study box. The coefficient $\overline{\beta}/\overline{\alpha}$ converts the salinity gradient into temperature units:

$$\frac{\overline{\beta}}{\overline{\alpha}} = \frac{\frac{1}{\rho} \cdot \left(\frac{\partial \rho}{\partial S}\right)_T}{-\frac{1}{\rho} \cdot \left(\frac{\partial \rho}{\partial T}\right)_S} \tag{20}$$

$\overline{\beta}/\overline{\alpha}$ was calculated for the average salinity and temperature of the boundary between t_1 and t_2.

There is an error related to the list of basic assumptions necessary to build–up the 2D box model, which affects the accuracy of the estimation. This error can only be assessed through validation with other method to estimate water fluxes (current meters, ADCP...) or any external variable —independent to the model—

able to control water circulation in the embayment. In the case of the 'Rías Baixas', the Ekman Transport ($-\overline{Q}_X$) will be used to validate the water fluxes produced by the model (see results section).

In addition, there is an error associated with the precision of the measured variables to calculate water fluxes (ε_Q) that can be estimated as:

$$\varepsilon_Q = \varepsilon_{QS} \cdot (1 - \overline{w}) + \varepsilon_{QT} \cdot \overline{w} \tag{21}$$

$$\varepsilon_{QS} = \frac{\varepsilon_R \cdot \overline{S}_B + \varepsilon_D + \left|(Q_S)_S\right| \cdot 2\varepsilon_S}{\left|\overline{S}_B - \overline{S}_S\right|} \tag{22}$$

$$\varepsilon_{QT} = \frac{\varepsilon_R \cdot \left|\overline{T}_B - \overline{T}_R\right| + \varepsilon_D + \varepsilon_H + \left(\left|(Q_S)_T\right| + \overline{R}\right) \cdot 2\varepsilon_T}{\left|\overline{T}_B - \overline{T}_S\right|} \tag{23}$$

Where ε_{QS} and ε_{QT} are the analytical errors of $(\overline{Q}_S)_S$ and $(\overline{Q}_S)_T$ respectively. ε_S and ε_T are the analytical errors of S_S or S_B (±0.005) and T_S, T_B or T_R (±0.005 °C). ε_R, ε_H and ε_D are the analytical errors of $R+P-E$ (~10%), H (~10%) and $\Delta S/\Delta t$ ($=2\varepsilon_S/\Delta t$) or $\Delta T/\Delta t$ ($=2\varepsilon_T/\Delta t$).

The average vertical advection fluxes between two consecutive surveys —$\overline{Q}_{Zi}$ and $\overline{Q}_{Zo}$ (Fig. 1c)— can be easily calculated once $\overline{Q}_{B1}$, $\overline{Q}_{B3}$ and $\overline{Q}_{B4}$ are known:

$$\overline{Q}_{Zi} = \overline{Q}_{B3} - \overline{Q}_{B1} - \overline{Q}_{Ei} = \overline{Q}_{B3} - \overline{Q}_{B1} - \frac{\Delta V_{Bi}}{\Delta t} \tag{24}$$

$$\overline{Q}_{Zo} = \overline{Q}_{B4} - \overline{Q}_{B3} - \overline{Q}_{Eo} = \overline{Q}_{B4} - \overline{Q}_{B3} - \frac{\Delta V_{Bo}}{\Delta t} \tag{25}$$

And the corresponding analytical errors are:

$$\varepsilon_{QZi} = \varepsilon_{Q3} + \varepsilon_{Q1} \tag{26}$$

$$\varepsilon_{QZo} = \varepsilon_{Q4} + \varepsilon_{Q3} \tag{27}$$

Since the error of $\Delta V_{Bi}/\Delta t$ or $\Delta V_{Bo}/\Delta t$ is negligible compared with ε_{Q1}, ε_{Q3} and ε_{Q4}.

Finally, the average vertical mixing fluxes between two consecutive surveys — $\overline{M}_{Zi}$ and $\overline{M}_{Zo}$ (Fig. 1c) — have to be calculated as:

$$M_{Zi} = \left(\overline{M}_{Zi}\right)_S \cdot \left(1 - \overline{w}_i\right) + \left(\overline{M}_{Zi}\right)_T \cdot \overline{w}_i \tag{28}$$

$$M_{Zo} = \left(\overline{M}_{Zo}\right)_S \cdot \left(1 - \overline{w}_o\right) + \left(\overline{M}_{Zo}\right)_T \cdot \overline{w}_o \tag{29}$$

With $\left(\overline{M}_{Zi}\right)_S$ and $\left(\overline{M}_{Zi}\right)_T$ being:

$$\left(\overline{M}_{Zi}\right)_S = \frac{V_{Bi} \cdot \frac{\Delta S_{Bi}}{\Delta t} + \left(\overline{S}_{Bi} - \overline{S}_{Zi}\right) \cdot \frac{\Delta V_{Bi}}{\Delta t} - \left(\overline{S}_{B3} - \overline{S}_{Zi}\right) \cdot \overline{Q}_{B3} + \left(\overline{S}_{B1} - \overline{S}_{Zi}\right) \cdot \overline{Q}_{B1}}{\left|\overline{S}_{Si} - \overline{S}_{Bi}\right|} \tag{30}$$

$$\left(M_{Zi}\right)_T = \frac{V_{Bi} \cdot \frac{\Delta T_{Bi}}{\Delta t} + \left(\overline{T}_{Bi} - \overline{T}_{Zi}\right) \cdot \frac{\Delta V_{Bi}}{\Delta t} - \left(\overline{T}_{B3} - \overline{T}_{Zi}\right) \cdot \overline{Q}_{B3} + \left(\overline{T}_{B1} - \overline{T}_{Zi}\right) \cdot \overline{Q}_{B1}}{\left|\overline{T}_{Si} - \overline{T}_{Bi}\right|} \tag{31}$$

And the corresponding errors:

$$\varepsilon_{MZi} = \varepsilon_{MZiS} \cdot \left(1 - \overline{w}_i\right) + \varepsilon_{MZiT} \cdot \overline{w}_i \tag{32}$$

$$\varepsilon_{MZiS} = \frac{\left(\left|\left(\overline{M}_{Zi}\right)_S\right| + 2 \cdot \frac{\overline{V}_{Bi}}{\Delta t} + \left|\overline{Q}_{B1}\right| + \left|\overline{Q}_{B3}\right|\right) \cdot 2\varepsilon_S + \left|\overline{S}_{B3} - \overline{S}_{Zi}\right| \cdot \varepsilon_{Q3} + \left|\overline{S}_{B1} - \overline{S}_{Zi}\right| \cdot \varepsilon_{Q1}}{\left|\overline{S}_{Bi} - \overline{S}_{Si}\right|} \tag{33}$$

$$\varepsilon_{MZiT} = \frac{\left(\left|\left(\overline{M}_{Zi}\right)_T\right| + 2 \cdot \frac{\overline{V}_{Bi}}{\Delta t} + \left|\overline{Q}_{B1}\right| + \left|\overline{Q}_{B3}\right|\right) \cdot 2\varepsilon_T + \left|\overline{T}_{B3} - \overline{T}_{Zi}\right| \cdot \varepsilon_{Q3} + \left|\overline{T}_{B1} - \overline{T}_{Zi}\right| \cdot \varepsilon_{Q1}}{\left|\overline{T}_{Bi} - \overline{T}_{Si}\right|} \tag{34}$$

Equivalent equations can be written for $\overline{M}_{Zo}$. Table 1 summarises the average errors of the convective and diffusive fluxes at each boundary and box during the four study periods. The direct calculation of $\overline{Q}_S$ and $\overline{Q}_B$ for the three boundaries produces the lowest analytical errors. Obviously, errors increase when $\overline{Q}_Z$ for the inner and outer box are calculated because they are derived from $\sum \overline{Q}_S$ (eqs 24–27). Finally, maximum analytical errors are associated to the complex estimation of $\overline{M}_Z$ at the inner and outer boxes, which includes $\sum \overline{Q}_S$ and $\overline{Q}_Z$ in the calculation (eqs. 28–34). It is worth noting that the values of ε_Q, ε_{QZ} and ε_{MZ} have to be considered as the maximum expected errors associated to the box–model estimation. However, the proper error of such estimations is probably much lower because of the averaging effect of all terms and properties involved in the calculations on the individual errors (Matsukawa & Suzuki, 1985).

Results

Thermal *versus* haline control of the density gradient

Box models calculate convective fluxes from salinity and temperature gradients. Equations (16) and (17) indicate that the resulting $\overline{Q}_S$ values —and consequently $\overline{Q}_B$ and $\overline{Q}_Z$— depend primarily on the vertical gradients of salinity ($\Delta\overline{S} = \overline{S}_B - \overline{S}_S$) and temperature ($\Delta\overline{T} = \overline{T}_B - \overline{T}_S$) and the thermohaline characteristics ($\overline{\beta}/\overline{\alpha}$) of the ría.

Figure 2 shows the short–time evolution of $(\overline{\beta}/\overline{\alpha})^2$, $\overline{w}$, $\Delta\overline{S}$ and $\Delta\overline{T}$ for the middle Ría of Vigo (stn 3; Fig 1b) during the four study periods. The dimensionless coefficient $(\overline{\beta}/\overline{\alpha})^2$ varies between 10.8 and 12.6 (Fig. 2a). When the three boundaries (inner, middle and outer) are considered the range of $(\overline{\beta}/\overline{\alpha})^2$ expands slightly from 9.7 to 12.9 (not shown). Therefore, the contribution of $(\overline{\beta}/\overline{\alpha})^2$ to the extremely large variability of $\overline{Q}_S$ —which expands three orders of magnitude— is not significant. The obtained range of $(\overline{\beta}/\overline{\alpha})^2$ indicates that the influence of salinity on the density gradient is one order of magnitude larger than the influence of temperature. This is a consequence of the water masses composition of the 'Rías Baixas',

mainly ENACW modified by heating across the sea–surface and freshening from continental runoff (Prego & Fraga, 1992; Rosón et al., 1997).

It is worth noting that $\overline{w}$ values were >0.5 during the spring, summer and autumn periods (Fig. 2a), indicating that density gradients in the middle Ría of Vigo were controlled by $\Delta\overline{T}$. During the summer and autumn surveys $\overline{w}$ was >0.88. On the contrary, density gradients during the winter survey, and therefore $\overline{Q_S}$, were controlled by $\Delta\overline{S}$ with $\overline{w}$ values <0.02. Obviously, $\overline{w}$ displayed important spatial differences (not shown). $\overline{w}$ decreased towards San Simon Bay during the periods of thermal control: it ranged from 0.01 to 0.28 during spring, 0.12 to 0.49 during summer and 0.60 to 0.77 during autumn. The reason behind the thermal control on the density gradients in the central Ría of Vigo during the spring, summer and autumn periods appears very clear in Figure 2b. Whereas the salinity gradients were <0.32 (spring), <0.34 (summer) and <0.17 (autumn), the temperature gradients (absolute values) were >0.80 °C, >2.01°C and >1.52°C for the corresponding periods. On the contrary, marked temperature inversion occurred during the winter period. The expected vertical homogenisation was prevented by extreme salinity gradients ranging from 0.83 to 3.07.

Steady–state *versus* non–steady–state control of horizontal exchange fluxes

Equation (18) calculates $\overline{Q}_S$ at any of the three study boundaries (1, 3 and 4; Figs. 1a, b). If $\Delta S/\Delta t$ in eq. (16) and $\Delta T/\Delta t$ in eq. (17) were equalled to zero —*i.e.* if the ría is left in steady–state from t_1 to t_2— the resulting steady–state term of $\overline{Q}_S$ is:

$$\left(\overline{Q}_S\right)_{SS} = \frac{\overline{R}\cdot\overline{S}_B}{\overline{S}_B-\overline{S}_S}\cdot(1-\overline{w}) + \frac{\overline{R}\cdot\left(\overline{T}_B-\overline{T}_R\right)-\overline{H}}{\overline{T}_B-\overline{T}_S}\cdot\overline{w} \qquad (35)$$

And, therefore, the corresponding non–steady–state term is:

$$\left(\overline{Q}_S\right)_{NSS} = \frac{V\cdot\frac{\Delta\overline{S}}{\Delta t}}{\overline{S}_B-\overline{S}_S}\cdot(1-\overline{w}) + \frac{V\cdot\frac{\Delta\overline{T}}{\Delta t}}{\overline{T}_B-\overline{T}_S}\cdot\overline{w} \qquad (36)$$

Figure 3 shows the time evolution of $\overline{Q}_S$ (eq. 18), the steady–state term of $\overline{Q}_S$ (eq. 35) and the non–steady–state term of $\overline{Q}_S$ (eq. 36) for boundary 3 (Fig. 1c). The short–time scale evolution of $\overline{Q}_S$ (in 10^3 m^3 s^{-1}) is clearly coupled to the non–steady–state term that, in turns, is secondarily controlled by the short–time scale changes in the net accumulation of salinity ($\Delta S/\Delta t$) and temperature ($\Delta T/\Delta t$):

$$\overline{Q}_{S3}\ (\pm 0.26) = 0.70\ (\pm 0.06) + 0.90\ (\pm 0.05)\cdot\left(\overline{Q}_{S3}\right)_{NSS} \qquad (37)$$

$$n = 18,\ r = +0.97$$

Therefore, the short–time–scale circulation pattern of the middle Ría of Vigo can be approached by a simple linear combination of a residual term (y–intercept, 0.70 10^3 m^3 s^{-1}) and a $\left(\overline{Q}_S\right)_{NSS}$ dependent term that controls the observed variability (slope, 0.90±0.05). The control of the non–steady–state term on the variability of $\overline{Q}_S$ clearly increases from the inner to the outer boundary (Table 2). More than 95% of the

variability of the exchange fluxes in the middle and outer ría can be explained by the non–steady–state term. Conversely, 96% of the variability of exchange fluxes in the inner ría depends on the steady–state term.

Dependence of fluxes on external forces. The key influence of the Ekman transport

The short–time–scale variability of $\overline{Q}_S$ at boundary 3 ($\overline{Q}_{S3}$) is parallel to the changes observed in the east–west component of the Ekman transport, $-\overline{Q}_X$ (Fig. 4; reg. 1 in Table 3). When $\overline{Q}_{S3}$ is correlated with $-\overline{Q}_X$ and $\overline{R}$, the correlation coefficient improves slightly (reg. 2 in Table 3). The heat exchange term ($\overline{H}$) does not contributes significantly to the short–time–scale variability of $\overline{Q}_{S3}$. The coefficient of $-\overline{Q}_X$ (2.3±0.2 km) represents the linear segment of coast where the Ekman transport should occur to produce the observed exchange flux. The wideness of the surface layer in the middle Ría of Vigo is 2.2 km, a value quite comparable with the coefficient obtained from reg. 2. This agreement indicates that the middle ría is under the direct influence of shelf wind–stress, which causes a dramatic enhancement of the weak positive circulation pattern induced by the river flux under upwelling conditions ($-\overline{Q}_X > 0$). On the contrary, under downwelling conditions ($-\overline{Q}_X < 0$) reversal of the circulation occurs when $\overline{Q}_X > 16(\pm4)/2.3(\pm0.2) \times \overline{R} = 7 (\pm2) \times \overline{R}$.

The average July 1987–96 R and $-Q_X$ for the Ría of Vigo were 9 $m^3 s^{-1}$ and 370 $m^3 s^{-1} km^{-1}$ of coast (Nogueira et al. 1997; Nogueira 1998). Therefore, the average $\overline{Q}_{S3}$ would be 1.0 10^3 $m^3 s^{-1}$, 14% due to $\overline{R}$ and 86% due to $-\overline{Q}_X$ in the middle of the upwelling season. On the contrary, the average December 1987–96 $\overline{R}$ and $-\overline{Q}_X$ were 35 $m^3 s^{-1}$ and –660 $m^3 s^{-1} km^{-1}$, which originated an average $\overline{Q}_{S3}$ of –0.96 10^{-3} $m^3 s^{-1}$ despite large $\overline{R}$ tended to produce a surface outflow of 0.56 10^{-3} $m^3 s^{-1}$. Note that the average $\overline{Q}_X / \overline{R}$ is as large as 19.

The evolution of the average annual cycles of $\overline{V}_y$ and $\overline{R}$ for the period 1987–96 (taken from Nogueira et al., 1997; Nogueira, 1998) over the $\overline{Q}_{S3}$ isolines defined by these variables with eq. (1) and reg. 2 (Table

3) is shown in Figure 5. December coincided with the period of maximum $\overline{V}_y$ (>6 m s^{-1}, southerly winds) and $\overline{R}$ (>35 m^3 s^{-1}), producing maximum average reversed fluxes of –1.0 10^3 m^3 s^{-1}. Both $\overline{V}_y$ and $\overline{R}$ diminished during January and February, resulting in a net decrease of the reversed fluxes in the middle ría. The circulation pattern became positive at the beginning of March, despite $\overline{V}_y$ was still >3m s^{-1} because of the flushing effect of $\overline{R}$ >22 $m^3 s^{-1}$. During March, $\overline{R}$ maintained at ~20 m^3 s^{-1} whilst a dramatic change was observed in $\overline{V}_y$ from >3 m s^{-1} to < –3 m s^{-1}, *i.e.* rapid transition from predominantly southerly to northerly winds occurred. As a consequence, the circulation pattern became strongly positive producing $\overline{Q}_{S3}$ values > 0.5 10^3 m^3 s^{-1}. From middle May to late August, both $\overline{R}$ and $\overline{V}_y$ decreased. Average $\overline{Q}_{S3}$ maintained at 1.0 10^3 m^3 s^{-1} during this 3 month period. The transition from predominantly northerly to southerly winds occurred by October. Finally, increased $\overline{R}$ during the autumn slightly counteracted the circulation reversal associated to increased $\overline{V}_y$. Therefore, reversed $\overline{Q}_{S3}$ values were lower during the autumn → winter transition that during the winter →spring transition.

We applied our method to calculate water fluxes to other data collected in the middle Ría of Vigo in April, July and September 1993 and March 1994 (data taken from Gómez–Fermín, 1995) and in the middle Ría of Arousa from May to October 1989 (data taken from Rosón et al., 1997). The middle Ría of Arousa (Fig. 1a) is 2.5 km wide, approximately the same as the middle Ría of Vigo. The multiple linear correlation of $\overline{Q}_S$ with $\overline{R}$ and $-\overline{Q}_X$ yields the equation (Fig. 6):

$$\overline{Q}_{S3}\ (\pm 1.5) = 20\ (\pm 6)\ 10^{-3} \cdot \overline{R} - 2.5\ (\pm 0.2)\ 10^{-3} \cdot \overline{Q}_X$$
$$n = 83,\ r = 0.81 \qquad (38)$$

This correlation is not significantly different from reg. 2 (Table 3) and supports the general statement that circulation in the central part of the Rías Baixas is under the direct influence of shelf wind–stress.

Comparison of eq. (37) and reg. 1 (Table 3) indicates that the Ekman transport controls horizontal exchange fluxes in the middle Ría of Vigo by acting on the non–steady–state component of the flux, *i.e*. on the $\Delta S/\Delta t$ and $\Delta T/\Delta t$ terms. The correlation coefficients presented in Table 3 clearly confirm this point for the outer and middle boundaries. This is the expected behaviour because during an upwelling event the cold and salty ENACW enters the rías in the bottom ingoing flux and the relatively warmer and fresher water in the ría is flushed out in the surface outgoing flux. Therefore, upwelling produces $\Delta S/\Delta t>0$ and $\Delta T/\Delta t<0$ that tend to reinforce the positive circulation pattern (eq. 36). On the contrary, during a downwelling event warm shelf surface water enters the ría in the surface ingoing flux and the relatively colder water into the ría is flushed out in the bottom outgoing flux. So, downwelling produces $\Delta T/\Delta t>0$ that tends to reverse the positive circulation pattern.

Table 3 also indicates that the short–time scale evolution of $\overline{Q}_{S4}$ is coupled with $-\overline{Q}_X$, as expected (r = 0.87). The coefficient of $-\overline{Q}_X$ is 10±2 km, which coincides again with the distance between Capes Subrido and Lamela, at the mouth of the Ría of Vigo (Fig. 1b). Consequently, the whole volume of oceanic ENACW upwelled in the segment of shelf off the mouth of the Ría of Vigo enters the embayment and returns to the shelf in the surface outgoing flux (modified by heating and freshening). On the light of eq. (38) this is likely applicable to the four Rías Baixas. On the other hand, the correlation between $\overline{Q}_{S1}$ and $-\overline{Q}_X$ is not significant.

Spatial variability of the circulation pattern under exemplar meteorological conditions

As demonstrated in the previous section, the short–time–scale variability of water fluxes in the Ría of Vigo is controlled by the external forces acting on the system: river flux at the eastern end of the ría and shelf wind–stress at the western end. Therefore, clear spatial differences should be observed in the circulation pattern. The ría will be studied under five contrasting meteorological conditions: **1**) spring downwelling; **2**) summer upwelling; **3**) autumn wind calm; **4**) winter upwelling and **5**) winter downwelling.

A downwelling event occurred from 7 to 10 April 1997 (Fig. 7a). Reversal of the positive circulation took place at the outer and middle boundaries, whereas circulation at the inner boundary was positive. Convergence of the reversed circulation in the outer ría and the positive circulation in the inner ría occurred at the inner box. As a consequence, the flushing time in the inner box (0.50 km^3) was 5.5 days, very large when compared with the 4.1 days in the much larger outer box (2.26 km^3). As much as 83% of the volume of shelf surface water which entered the ría was advected downwards in the outer box, 4% was used to expand downwards the surface layer of the outer box and the remaining 13% was advected into the surface layer of the inner box. Convergence at the inner volume produced that 84% of the volume entering the surface layer (71% from the outer ría, 29% from San Simón Bay) was advected downwards to the bottom layer.

During the summer upwelling event from 15 to 18 July 1997 (Fig. 7b) circulation was positive throughout the ría, although water fluxes in the inner boundary did not indicate enhancement by upwelling. This was also suggested by the lack of correlation between $\overline{Q}_{S1}$ and $\left(\overline{Q}_{S1}\right)_{NSS}$ (Table 2). Flushing times during this upwelling event were 3.0 and 3.6 days in the inner and outer boxes, respectively. Upwelling in the outer and middle ría represented 75% and 92% of the bottom ingoing flux. The abrupt bathymetry change in the surroundings of stn 3 is likely the responsible for the enhancement of upwelling in the inner box. This behaviour was also observed by Rosón et al. (1997) in the adjacent Ría of Arousa.

Water circulation was extremely slow during the autumn wind calm from 25 to 29 September 1997 (Fig. 7c). This can be considered the expected circulation pattern of the Rías Baixas in the absence of shelf wind–stress. Flushing times of 11 and 130 days were calculated for the inner and outer boxes. Comparison of this event with the other four selected periods, proves the key role played by shelf wind–stress in water circulation of the Rías Baixas.

The winter upwelling event illustrates the effect of northerly winds from 1 to 5 December 1997 (Fig. 7d), in the middle of the downwelling season. Upwelling reinforced the positive circulation pattern generated by continental runoff (50 $m^3\ s^{-1}$), producing fluxes larger than those recorded during the summer upwelling event. Flushing times during this period reduced to 2.5 and 2.8 days in the inner and outer ría, respectively.

Haline stratification associated to large continental runoff limited upwelling in the outer and inner volumes to 67% and 74% of the bottom ingoing flux.

Finally, the winter downwelling event from 8 to 11 December 1997 (Fig. 7e) is a typical example of the effect of strong southerly winds in the Rías Baixas. Extreme reversal of the circulation pattern was observed, affecting the outer, middle and inner boundaries. Therefore, shelf surface waters penetrated up to San Simon Bay, where water fluxes were low despite large continental runoff in the winter period (Fig. 4). Flushing times during this event reduced to 1.4 and 1.7 days in the outer and inner boxes respectively. Downwelling represented 76% and 94% of the surface ingoing flux in the outer and inner boxes. The abrupt bathymetry change was again the reason behind enhanced downwelling in the inner box.

Discussion

2D box model approach to the water circulation of a coastal embayment affected by upwelling

Box models have been successfully applied to study circulation patterns, flushing times of pollutants and budgets of reactive species in well–mixed (1D approach; e.g. Stommel 1953; Boyle et al., 1974; Miller & McPherson, 1991; Smith et al., 1991; Simpson & Rippeth, 1998) and partially–mixed (2D approach; eg. Pritchard, 1969; Taft et al., 1976; Officer, 1980) estuaries, embayments and enclosed seas. Steady–state conditions have been assumed in all these studies. This assumption implies that the volumes and the thermohaline and chemical characteristics of the ingoing and outgoing fluxes remain unchanged for a period equivalent to the calculated flushing time. However, coastal upwelling areas are highly dynamic systems where dramatic hydrographic changes occur at short time intervals. Steady–state box models (Otto, 1975; González et al., 1979; Prego et al., 1990; Ríos, 1992; Prego & Fraga, 1992) fail to solve the high frequency of the wind stress/relaxation sequence in the NW Iberian Upwelling System, which describes a complete cycle in 14±4 days (Álvarez–Salgado et al., 1993). A non–steady–state approach is mandatory in this case. Non–steady–state box models have also been applied by Matsukawa & Suzuki (1985) and Suzuki & Matsukawa (1987) for two bays in Japan and by Smith & Hollibaugh (1997) to Tomales Bay, California. We have demonstrated that >95% of the variability in the middle and outer ría depends on the non–steady–state

term of the flux. In turns, Ekman pumping controls >75% of the variability of the non–steady–state term. Enhanced vertical advection in the Ría of Vigo was pointed out for the first time by Margalef & Andreu (1958) and it was related with shelf winds by Anadón (1958). The importance of events on the shelf in driving the motion within estuaries and bays has been widely recognised since the middle 70's (Carter et al., 1979), although it is quite unusual that >75% of the total variance is associated with an external force. For example, Elliot (1978) showed that only 25% of the variance in the Potomac Estuary was due to the Ekman flux in the coast.

Flux calculations are robust in estuaries, bays and enclosed seas where horizontal (1D approach) or vertical (2D approach) salinity gradients are large enough; at least 25 times the analytical error of ΔS (= $2 \cdot \varepsilon_S$ = 0.01). However this is not the case in many coastal systems, mainly during the summer period when continental runoff reduces to extreme minimum values. In fact, Smith & Hollibaugh (1997) found empirically that salinity differences <0.3 resulted in anomalously large fluxes that they rejected. Inspired by Rahm & Wulff (1992), Rosón et al. (1997) used parallel salinity and temperature profiles to estimate water fluxes in the Ría of Arousa during the upwelling season. In the present work, we simplified Rosón et al.'s (1997) calculations and introduce an objective weighting factor, $\overline{w}$, based on the ratio of the coefficients of thermal expansion and haline contraction. Our results indicate that temperature is the best tracer of circulation in the study system during the spring, summer and autumn periods. In this sense, Minas et al. (1986) used heat budgets to roughly estimate flushing times in the upwelling systems of NW Africa, California and Perú.

It is also interesting to note that our non–steady–state approach considers time changes in the depth of the level of no motion, *i.e.* time changes in the volumes of the surface and bottom layers of each box, presenting $Q_E = \Delta V_B / \Delta t = -\Delta V_S / \Delta t$ as a new term to the water balance. This vertical component of the water balance use to be an order of magnitude lower than the convective fluxes. Finally, our 2D box model includes a rigorous assessment of the expected error of fluxes. We demonstrate that, despite the complex set of calculations involving measurements and estimation of many terms, the salinity–temperature weighted approach is able to keep the errors within acceptable levels of confidence.

Box model fluxes have never been simultaneously compared with current meter or ADCP measurements in the 'Rías Baixas'. However, conversion of our fluxes into velocities produce values consistent with those recorded from current meter arrays under comparable hydrographic conditions (Figueiras et al., 1994; Álvarez–Salgado et al., 1998). Anyway, results from direct current measurements indicate water displacements at a given position and depth within the embayment, whilst box model fluxes are representative for cross–sections and volumes of the order of 10^4 m^2 and 10^6 m^3 respectively. Rudimentary 3D (Taboada et al., 1998) and vertically integrated 2D (Gómez–Gesteira et al., 1999) hydrodynamic models have been recently developed for the Ría of Vigo. However, they still fail to predict net water displacements generated by the offshore Ekman transport because they surprisingly did not consider shelf wind–stress in their computations. More recently, Torres–López et al. (accepted) have developed a 3D non–linear baroclinic model able to produce water fluxes and thermohaline distributions in the Ría of Vigo (NW Spain) under contrasting upwelling and downwelling favourable wind conditions. They obtain circulation patterns consistent with the result from our 2D kinematic box model.

Shelf surface waters off the Rías Baixas: outwelling *versus* upwelling

Water circulation patterns in the middle an outer segment of the 'Rías Baixas' are controlled by shelf wind–stress. Therefore, the Rías 'Baixas' behave as extensions of the shelf rather than as proper estuaries. In fact, the rías are out of the classical hydrodynamic classification of estuaries into salt wedge, partially–mixed and well–mixed systems (Bowden, 1980; Beer, 1983). The Spanish rías must be defined 'like' estuaries not 'as' estuaries (Rosón et al., 1997). During the upwelling season they circulate 'like' partially mixed estuaries but they are forced by shelf wind–stress ('as' coastal upwelling systems) not by continental runoff ('as' estuaries). In addition, a reversal of the positive circulation pattern can occur under downwelling conditions. The ría would circulate 'like' a negative estuary in that case. In a proper estuary, negative circulation only would occur when $R+P-E<0$ (Beer, 1983), and this is never the case of the Spanish rías. Continental runoff to the rías is only important during the autumn–winter period, when these embayments have been classified 'as' estuaries (Prego & Fraga, 1992). However, our study proves that wind–stress over the shelf is still the key factor controlling the circulation pattern during the winter, in such a way that when $\overline{Q}_X / \overline{R} > 7$ circulation is reversed in the outer and middle ría despite the flushing effect of large continental runoff.

It is worth noting that the coefficient of $-\overline{Q}_X$ in regressions 2 & 5 (Table 3) coincides with the wideness of the rías of Vigo and Arousa at both the outer and middle boundaries. This proves that the whole volume of ENACW upwelled over the 200m isobath at the continental slope off the mouth of the four 'Rías Baixas' crosses the 50m isobath and enters the embayments (Fig. 1a). Therefore, none of this ENACW upwells between the 200m isobath and the mouth of the rías but it is returned to the shelf *via* the surface outgoing flux from the rías. Obviously, outwelled ENACW from the rías is warmer and fresher than pure upwelled ENACW. Modification of ENACW into the ría depends on the meteorological conditions ($\overline{R}$ and $\overline{H}$) and the residence time of water within the embayments. Both freshening and warming tend to increase the buoyancy of the surface outgoing flux, increasing stratification and preventing *in situ* upwelling. This case of 'upwelling shadowing' have been previously described by Tenore et al. (1995) to explain colder shelf surface water temperatures north of Cape Finisterre. However, these authors did not quantify the

phenomenon. Upwelling shadowing have been also described in the California upwelling system as a consequence of outwelling from Monterrey Bay (Graham, 1993).

The total volume of the four Rías Baixas is 13.65 km^3, with an average depth of 20m (Prego, 1990). Therefore, average flushing times within the rías for moderate ($-\overline{Q}_X$ = 500 $m^3\ s^{-1}\ km^{-1}$, $\overline{V}_y$ = –6 $m\ s^{-1}$), strong (1000 $m^3\ s^{-1}\ km^{-1}$, –8 $m\ s^{-1}$) and inclement (1500 $m^3\ s^{-1}\ km^{-1}$, –10 $m\ s^{-1}$) upwelling conditions are 14.5, 7.3 and 4.8 days respectively, considering that the mouth of the four rías comprises 43.5 km (Fig. 1a). Since the total length of the linear segment of coast between Cape Finisterre and the River Miño is 112.5 km, it results that ~40% of shelf surface waters off the rías consists of outwelled modified ENACW. The remaining ~60% has to be pure ENACW directly upwelled on the shelf. For comparison, the total volume of shelf waters inshore the 200m isobath amounts 243 km^3 and the average total flushing times for moderate, strong and inclement northerly winds are 50, 25 and 17 days. Therefore, 40% of the pure ENACW that upwells over the shelf passes through the limited volume of the rías (<6% of the total) before reaching the productive surface layer. The biogeochemical implications of outwelling during the upwelling season are important. **1**) Partial/total nutrient consumption and progressive stratification of ENACW upwelled into the ría produces that food webs on the shelf are probably in an advanced state of development compared with the actual upwelling conditions. In fact, phytoplankton assemblages in upwelling areas succeed from fast growing small chain–forming diatoms to slow growing large centric diatoms and, subsequently, small flagellates as they drift offshore (Barber & Smith, 1981; MacIsaac et al., 1985; Dugdale & Wilkerson, 1989). **2**) A considerable fraction of the organic materials produced into the rías are exported to the shelf, where large particles meet the organic (Lopez–Jamar et al., 1992) and opal (Prego & Bao, 1997) biodeposits and contribute to rapid ageing of upwelled ENACW (Álvarez–Salgado et al., 1993; 1997).

During the downwelling season, predominant southerly winds provoke surfacing of the compensation undercurrent characteristic of the upwelling period. A poleward slope flow of warm and salty subtropical water has been observed from Cape Saõ Vicente (37°N; Frouin et al., 1990) to the Armorican shelf (47°N; Pingree & Le Cann, 1990). Poleward surface currents of 0.1–0.2 $cm{\cdot}s^{-1}$ off the Rías Baixas (Haynes & Barton 1990; 1991) cause piling of ocean water on the shelf, which eventually enters the rías. This was the

situation following the strong reversal of circulation during the winter survey. The pattern is similar to that found in the California Current system; from August to November the poleward California Undercurrent gets stronger and shoals to the surface (Largier et al., 1993; Bray & Greengrove, 1993). Average 1987–96 continental runoff to the Ría of Vigo from October to March was 30 m^3 s^{-1}. Therefore, for southerly winds > 3.7 m s^{-1}, ~40% of the surface water piled on the shelf between Cape Finisterre and River Miño enters into the 'Rías Baixas' and it is returned to the shelf through the bottom outgoing flux.

Acknowledgements

The authors wish to thank the captain and crew of '*R/V Mytilus*' and the members of the IIM Group of Oceanography for their help during the sampling programme. Financial support for this work came from CICYT Grant No. AMB95–1084. Fellowships from the Spanish 'Ministerio de Educación y Ciencia' funded J. Gago and B.M. Míguez to carry out this work.

References

Álvarez–Salgado, X.A., Rosón, G., Pérez, F.F. & Pazos, Y. 1993. Hydrographic variability off the Rías Baixas (NW Spain) during the upwelling season. *Journal of Geophysical. Research* **98**, 14447–14455.

Álvarez–Salgado, X.A., Rosón, G., Pérez, F.F., Figueiras, F.G. & Pazos, Y. 1996. Nitrogen cycling in an estuarine upwelling system, the Ría de Arousa (NW Spain). I: short–time–scale evolution of hydrodynamic and biogeochemical circulation of nitrogen species. *Marine Ecology Progress Series* **135**, 259–273.

Álvarez–Salgado, X.A., Castro, C.G., Pérez, F.F. & Fraga, F. 1997. Nutrient mineralization patterns in shelf waters of the Western Iberian upwelling. *Continental Shelf Research* **17**, 1247–1270.

Álvarez–Salgado, X.A., Figueiras, F.G., Villarino, M.L. & Pazos, Y. 1998. Hydrodynamics and chemical conditions during onset of a red tide assemblage in an estuarine upwelling ecosystem. *Marine Biology* **130**, 509–519.

Anadón, E. (1958). Las Corrientes Marinas en la Ría de Vigo. *Industria Pesquera* **745–746**, 58–59.

Bakun, A. & Nelson, C.S. 1991. The seasonal cycle of wind–stress curl in subtropical eastern boundary current regions. *Journal of Physical Oceanography* **21,** 1815–1834.

Barber, R.T. & Smith, R.L. 1981. Coastal upwelling ecosystems, p. 31–68. *In* A.R. Longhurst [ed.], Analysis of Marine Systems. Academic Press, San Diego.

Beer, T. 1983. *Environmental Oceanography*. Pergamon Press, Oxford, 262 p.

Boyle, E., Collier, R, Dengler, A.T., Edmond, J.M., Ng, A.C. & Stallard, R.F. 1974. On the Chemical Mass Balance of Estuaries. *Geochimica Cosmochimica Acta*, **38** 1719–1728.

Bowden, K.F. 1980. Physical factors: salinity, temperature, circulation and mixing processes. In Chemistry and Biogeoqchemistry of Estuaries (Olauson, E. & Cato, I., eds.) John Wiley and Sons, Chichester, pp 37–70.

Bray, N.A., & Greengrove, C.L. 1993. Circulation over the shelf and slope off Northern California. *Journal of Geophysical Research* **98**, 18119–18145.

Carter, H.H., Najarin, T.O., Pritchard, D.W. & Wilson, R.E. 1979. The dynamics of motion in estuaries and other coastal water bodies. *Reviews of Geophysics and Space Physics* **17**, 1585–1590.

Dugdale, R.C. & Wilkerson, F.P. 1989. New production in the upwelling center at Point Conception, California: Temporal and spatial patterns. *Deep–Sea Research* **36**, 985–1007.

Elliot, A.J. (1978). Observations of the meteorologically induced circulation in the Potomac Estuary. *Estuarine and Coastal Marine Science* **6**, 285–290.

Gómez–Fermín, E. 1995. *Acoplamiento Dinámico entre las Poblaciones de Microplancton y la Circulación en la Ría de Vigo (NO España).* Doctoral Thesis. University of Santiago de Compostela, 215 pp.

Gómez–Fermín, E., Figueiras, F.G., Arbones, B. & Villarino, M.L. 1996. Short–time scale development of a *Gymnodinium catenatum* population in the Ría de Vigo (NW Spain). *Journal Phycology* **32**, 212–221.

Figueiras, F.G., Jones, K.J., Mosquera, A.M., Álvarez–Salgado, X.A.& McDougall, N. 1994. Red tide assemblage formation in a estuarine upwelling ecosystem: Ría de Vigo. *Journal of Plankton Research* **16**, 857–878.

Fiúza, A.F.G. 1983. Upwelling patterns of Portugal, In *Coastal Upwelling: Its sediment record* (Suess, E. &Thiede, J., eds). Plenum Press, NY. pp. 85–97.

Fraga, F. 1981. Upwelling off the Galician coast, Northwest Spain. In *Coastal Upwelling. Coastal and Estuarine Sciences vol. 1* (Richards F.A., ed.). AGU, Washighton, D.C., pp. 176–182.

Frouin, R., Fiúza, A.F.G., Ambar, I. & Boyd, T.J. 1990. Observations of a poleward surface current off the coasts of Portugal and Spain during winter. *Journal of Geophysical Research* **95**, 679–691.

Graham, W.M. 1993. Spatio–temporal scale assessment of an 'upwelling shadow' in Northern Monterey Bay, California. *Estuaries* **16**, 83–91.

Gómez–Gesteira, M., Montero, P., Prego, R., Taboada, J.J., Leitao, P., Ruiz–Villareal, M., Neves, R. & Pérez–Villar, V. 1999. A two–dimensional particle tracking model for pollution dispersion in A Coruña and Vigo Rias (NW Spain). *Oceanologica Acta* **22**, 167–177.

González, N., González, J.J., García, C. & Cabanas, J.M. 1979. Dinámica de Nutrientes en las Rías de Arosa y Muros (NW España). *Boletín del Instituto Español de Oceanografía* **V,** 51–79.

Haynes, R. & Barton, E.D. 1990. A poleward flow along the Atlantic coast of the Iberian Peninsula. *Journal of Geophysical Research* **95**, 11425–11441.

Haynes, R. & Barton, E.D. 1991. Lagrangian observations in the Iberian Coastal Transition Zone. J. *Journal of Geophysical Research* **96**, 14731–14741.

Hidy G.M. 1972. A view of recent air–sea interaction research. *Bulletin of the American Meteorological Society* **53**, 1083–1102.

Laevastu, T. 1963. Energy exchange in the North Pacific, its relations to weather and its oceanographic consequences. Part 1: Formulas and monograms for computation of heat exchange components over the sea. Hawaian Institute for Geophysical Research. Report 29:15.

Largier, J.L., Magnell, B.A. & Winant, C.D. 1993. Subtidal circulation over the Northern California Shelf. *Journal of Geophysical Research* **98**, 18147–18179.

López–Jamar, E., Cal., R.M., González, G., Hanson, R.B., Rey, J., Santiago, G. & Tenore, K.R. 1992. Upwelling and outwelling effects on the benthic regime of the continental shelf off Galicia, NW Spain. *Journal of Marine Research* **50**, 465–488.

Margalef, R. & Andreu B. 1958. Componente Vertical de los Movimientos de Agua en la Ría de Vigo y su Posible Relación con la Entrada de la Sardina. *Investigación Pesquera* **11**, 105–126.

MacIsaac, J.J., Dugdale, R.C., Barber, R.T., Blasco, D., & Packard, T.T. 1985. Primary production cycle in an upwelling center. *Deep–Sea Research* **32**, 503–529.

Matsukawa, Y. & Suzuki, T. 1985. Box model analysis of hydrographic behaviour of nitrogen and phosphorus in a eutrophic estuary. *Journal of the Oceanographic Society of Japan* **41,** 407–426.

McClain, C.R., Chao, S.–Y. Atkinson, L.P., Blanton, J.O. & de Castillejo, F.F. 1986. Wind–driven upwelling in the vicinity of Cape Finisterre, Spain. *Journal of Geophysical Research* **91**, 8470–8486.

Miller, R.L. & McPherson, B.J. 1991. Estimating estuarine flushing and residence time in Charlotte Harbor, Florida, via salt balance and a box model. *Limnology and Oceanography* **36**, 602–612.

Minas, H.J., Minas, M. & Packard, T.T. 1986. Productivity in upwelling areas deduced from hydrographic and chemical fields. *Limnology and Oceanography* **31**, 1182–1206.

Nogueira, E., Pérez, F.F. & Ríos, A.F. 1997. Seasonal and long–term trends in an estuarine upwelling ecosystem (Ría de Vigo, NW Spain). *Estuarine, Coastal and Shelf Science* **44**, 285–300.

Nogueira, E. 1998. *Análisis y Modelado de la Variabilidad Temporal de las Características Hidrográficas en la Ría de Vigo*. Doctoral Thesis. University of Vigo, 238 pp.

Officer, C.B. 1980. Box models revisited. In *Estuarine and wetlands processes with emphasis on modelling* (Hamilton, P. & McDonald, K.B., eds.). Plenum Press, pp. 65–114.

Otto, L. 1975. *Oceanography of the Ría de Arousa (NW Spain)*. Konink. Meteor. International Medelingen en Verlan, No 96, 210 pp.

Pingree, R.D. & Le Cann, B. 1990. Structure , strength and seasonality of the slope currents in the Bay of Biscay region. *Journal of the Marine Biological Association of the U.K.* 70, 857–885.

Prego, R. 1990. Las sales nutrientes en las rías gallegas. *InformesTécnicos de Scientia Marina* **157**, 31pp.

Prego, R., Fraga, F. & Ríos, A.F. 1990. Water Interchange between the Ria of Vigo and the Continental Shelf. *Scientia Marina* **54**, 95–100.

Prego, R. & Fraga, F. 1992. A simple model to calculate the residual flows in a Spanish ría. Hydrographic consequences in the Ría of Vigo. *Estuarine, Coastal and Shelf Science* **34**, 603–615.

Prego, R. & Bao, R. 1997. Upwelling influence on the Galician coast: silicate in shelf waters and underlying surface sediments. *Continental Shelf Research* **17**, 307–318.

Pritchard, D.W. 1969. Dispersión and Flushing of Pollutants in Estuaries. *Journal Hydraulics Division American Society Civil Engineers* **95**, 115–124.

Rahm, L. & Wulff, F. 1992. Using Parallel Salinity and Temperature Profiles for Calculations of Estuarine Fluxes with Reference to the Baltic Proper. *Netherlands Journal of Sea Research* **29**, 281–289.

Ríos, A.F., Nombela, M.A., Pérez, F.F., Rosón, G. & Fraga, F. 1992. Calculation of Runoff to an Estuary. Ría de Vigo. *Scientia Marina* **56**, 29–33.

Ríos, A.F. (1992). *El fitoplancton de la Ría de Vigo y sus condiciones ambientales*. Doctoral Thesis. University of Santiago de Compostela, 416 pp.

Rosón, G., Álvarez–Salgado, X.A. & Pérez, F.F. 1997. A non stationary box model to determine residual fluxes in a partially mixed estuary, based on both thermohaline properties. Application to the Ria de Arousa (NW Spain). *Estuarine, Coastal and Shelf Science*, **44**, 249–262.

Schlesinger, W.H. 1997. *Biogeochemistry, an analysis of Global Change*. 2nd Edition. Academic Press, San Diego.

Simpson, J.H. & Rippeth, T.P. 1998. Non–conservative nutrient fluxes from budgets for the Irish Sea. *Estuarine Coastal and Shelf Science* **47**, 707–714.

Smith, S.V., Hollibaugh, J.T., Dollar, S.J. & Vink, S. 1991. Tomales Bay metabolism: C–N–P stoichiometry and ecosystem heterotrophy at the land–sea interface. *Estuarine, Coastal and Shelf Science* **33**, 223–257.

Smith, S.V. & Hollibaugh, J.T. 1997. Annual cycle and interannual variability of ecosystem metabolism in a temperate climate embayment. *Ecological Monographs* **67**: 509–533.

Stommel, H. (1953). Computation of Pollution in a Vertically Mixed Estuary. *Seawage and Industrial Wastes*, **25**: 1065–1071.

Suzuki, T. & Matsukawa, Y. 1987. Hydrography and budget of dissolved total nitrogen and dissolved oxygen in the stratified season in Mikawa Bay, Japan. *Journal of the Oceanographical Society of Japan* **43**, 37–48.

Taboada, J.J., Prego, R., Ruiz–Villareal, M., Gómez–Gesteira, M., Montero, P., Santos, A.P. & Pérez–Villar, V. 1998. Evaluation of the seasonal variations in the residual circulation in the Ría de Vigo (NW Spain) by means of a 3D baroclinic model. *Estuarine, Coastal and Shelf Science* **47**, 661–670.

Taft, J.L., Elliott, A.J. & Taylor, W.R. 1978. Box model analysis of Chesapeake by ammonium and nitrate fluxes. In *Estuarine Interactions* (Wiley, M.J., ed.). Academic press, pp. 115–130.

Tenore, K.R. and others. 1995. Fisheries and Oceanography off Galicia, NW Spain: Mesoscale spatial and temporal changes in physical processes and resultant patterns of biological productivity. Journal of Geophysical Research **100**, 10943–10966.

Torres–López, S., Varela, R. & Delhez, E. Influences of different wind conditions on the residual circulation and the thermohaline distribution of the Ría de Vigo (NW Spain): a 3–D hydrodynamical model. *Scientia Marina*, accepted.

UNESCO. 1985. *The international system of units (SI) in oceanography*. UNESCO technical papers in marine sciences **45**.

Walsh, J.J. 1991. Importance of continental margins in the marine biogeochemical cycling of carbon and nitrogen. Nature **359**, 53–55.

Wollast, R. 1998. The global coastal zone, processes and methods. In *The Sea* (Brink, K.H. & Robinson, A.R., eds.). New York, pp. 213–252.

Wooster, W.S., Bakun, A. & Mclain, D.R. 1976. The seasonal upwelling cycle along the eastern boundary of the North Atlantic. *Journal of Marine Research* **34**, 131–141.

Table 1. Percentage ($\varepsilon_X \div X \times 100$) and absolute value ($\pm\varepsilon_X$) of the error in the estimation of horizontal and vertical convective fluxes and vertical diffusive fluxes at each boundary (*1*, *3* and *4*) and box (*i* and *o*) during the four sampling periods (spring, summer, autumn and winter).

ε of	Spring	Summer	Autumn	Winter
$\overline{Q}_{B1}$, $\overline{Q}_{S1}$	14% (±90)	9% (±18)	11% (±34)	13% (±25)
$\overline{Q}_{B3}$, $\overline{Q}_{S3}$	17% (±116)	3% (±23)	12% (±30)	7% (±35)
$\overline{Q}_{B4}$, $\overline{Q}_{S4}$	16% (±373)	5% (±178)	20% (±251)	4% (±389)
$\overline{Q}_{Zi}$	62% (±206)	6 % (±41)	82% (±64)	9% (±160)
$\overline{Q}_{Zo}$	26% (±489)	7% (±201)	29% (±281)	7% (±524)
$\overline{M}_{Zi}$	48% (±415)	13% (±64)	18% (±136)	18% (±110)
$\overline{M}_{Zo}$	71% (±732)	19% (±232)	26% (±348)	12% (±424)

Table 2. Correlation coefficients (r^2) of the linear regressions between $\overline{Q}_S$ and the corresponding steady–state, $(\overline{Q}_S)_{SS}$, and non–steady–state, $(\overline{Q}_S)_{NSS}$, terms at the inner (1), middle (3) and outer (4) boundaries. The total volume of the ría delimited by each boundary (km^3) is also presented. NS, no significant; ***, $p< 0.001$.

	$(\overline{Q}_S)_{SS}$	$(\overline{Q}_S)_{NSS}$	V
Boundary 1	0.96***	0.09^{NS}	$34.5\ 10^{-3}$
Boundary 3	0.09^{NS}	0.95***	0.53
Boundary 4	0.01^{NS}	0.96***	2.80

Table 3. Selection of the significant linear regression equations relating $\overline{Q}_S$ and $(\overline{Q}_S)_{NSS}$ with the external forces acting on the study system, $\overline{R}$ and $-\overline{Q}_X$, at the inner (1) middle (3) and outer (4) boundary. In 10^3 m^3 s^{-1}. *r*, regression coefficient, n = 18.

	Equation	*r*
1	$\overline{Q}_{S3}$ (±0.59) = 0.2(±0.1) –2.4(±0.4) 10^{-3} $\cdot \overline{Q}_X$	0.86
2	$\overline{Q}_{S3}$ (±0.45) = 16(±4) $10^{-3}\cdot \overline{R}$ – 2.3(±0.2) $10^{-3}\cdot \overline{Q}_X$	0.92
3	$(\overline{Q}_{S3})_{NSS}$ (±0.66) = –0.6(±0.2) – 2.7(±0.4) $10^{-3}\cdot \overline{Q}_X$	0.87
4	$\overline{Q}_{S4}$ (±2.9) = –1.0(±0.8) –11(±2) $10^{-3}\cdot \overline{Q}_X$	0.84
5	$\overline{Q}_{S4}$ (±2.7) = –2.1(±0.9) +65(±35) $10^{-3}\cdot \overline{R}$ – 10(±2) $10^{-3}\cdot \overline{Q}_X$	0.87
6	$(\overline{Q}_{S4})_{NSS}$ (±3.0) = –3.2(±0.8) – 11(±2) $10^{-3}\cdot \overline{Q}_X$	0.83
7	$(\overline{Q}_{S4})_{NSS}$ (±2.8) = –4.3(±0.9) + 74(±36) $10^{-3}\cdot \overline{R}$ – 11(±2) $10^{-3}\cdot \overline{Q}_X$	0.87

Figure Captions

Figure 1. Chart of the study area, shelf waters of the NW Iberian upwelling system from Cape Finisterre to the River Miño (**a**). The position of the Meteorological observatory at Cape Finisterre is indicated (white square). Detailed map of the Ría of Vigo, showing the five sampling sites visited during 1997 (black circles) and the position of the Meteorological Observatory in Bouzas (white triangle) (**b**). Section across the central channel of the Ría the Vigo showing the two boxes —with surface and bottom layer— in which the embayment was divided (**c**). $R+P-E$, hydrological balance; Q_B and Q_S surface and bottom horizontal advective fluxes; Q_Z and M_Z, vertical advective and mixing fluxes; Q_E, change of volume of the bottom layer. Subscripts *1*, *3*, *4*, *i* and *o* refers to the inner, middle and outer boundaries and the inner and outer boxes.

Figure 2. Average values of $(\beta/\alpha)^2$ and w (**a**); and ΔS and ΔT (**b**) between two consecutive surveys during the four study periods in the Ría of Vigo during 1997.

Figure 3. Average value of Q_{S3}, the steady–state term of Q_{S3} and the non–steady–state term of Q_{S3} between two consecutive surveys during the four study periods in the Ría of Vigo during 1997.

Figure 4. Average value of R and $-Q_X$ (**a**); and Q_{S3} and estimated $Q_{S3}(R,-Q_X)$ with reg. 2 (Table 3) (**b**) between two consecutive surveys during the four study periods in the Ría of Vigo during 1997.

Figure 5. Time evolution of the average 1987–96 weekly value of R and Vy (circles) on the $\overline{Q}_{S3}$ isolines defined by $\overline{R}$ and $\overline{Vy}$ through eq. (1) and reg. 2 (Table 3).

Figure 6. X–Y plot of $\overline{Q}_S$ versus $-\overline{Q}_X$ in the middle Ría of Vigo during 1997 (black circles) and 1993–94 (white circles) and Ría of Arousa during 1989 (grey circles).

Figure 7. Average water fluxes ($\overline{Q}_S$, $\overline{Q}_B$, $\overline{Q}_Z$ and $\overline{M}_Z$) between two consecutive surveys at the three boundaries and two layers defined in the Ría of Vigo during five selected episodes: spring downwelling, April 7 to 10 (**a**); summer upwelling, July 15 to 18 (**b**); autumn wind calm, September 25 to 29 (**c**); winter upwelling, December 1 to 5 (**d**); and winter downwelling December 8 to 11 (**e**). Fluxes in 10^3 m^3 s^{-1}.

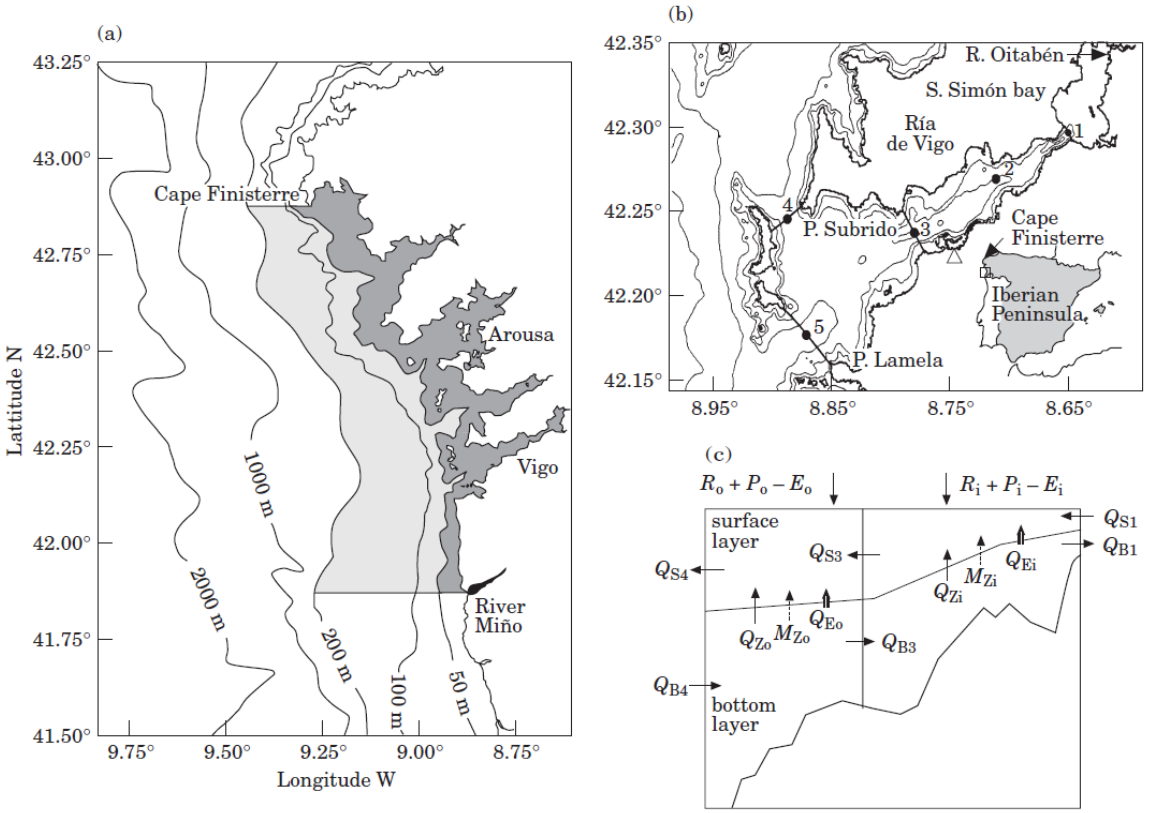

Figure 1

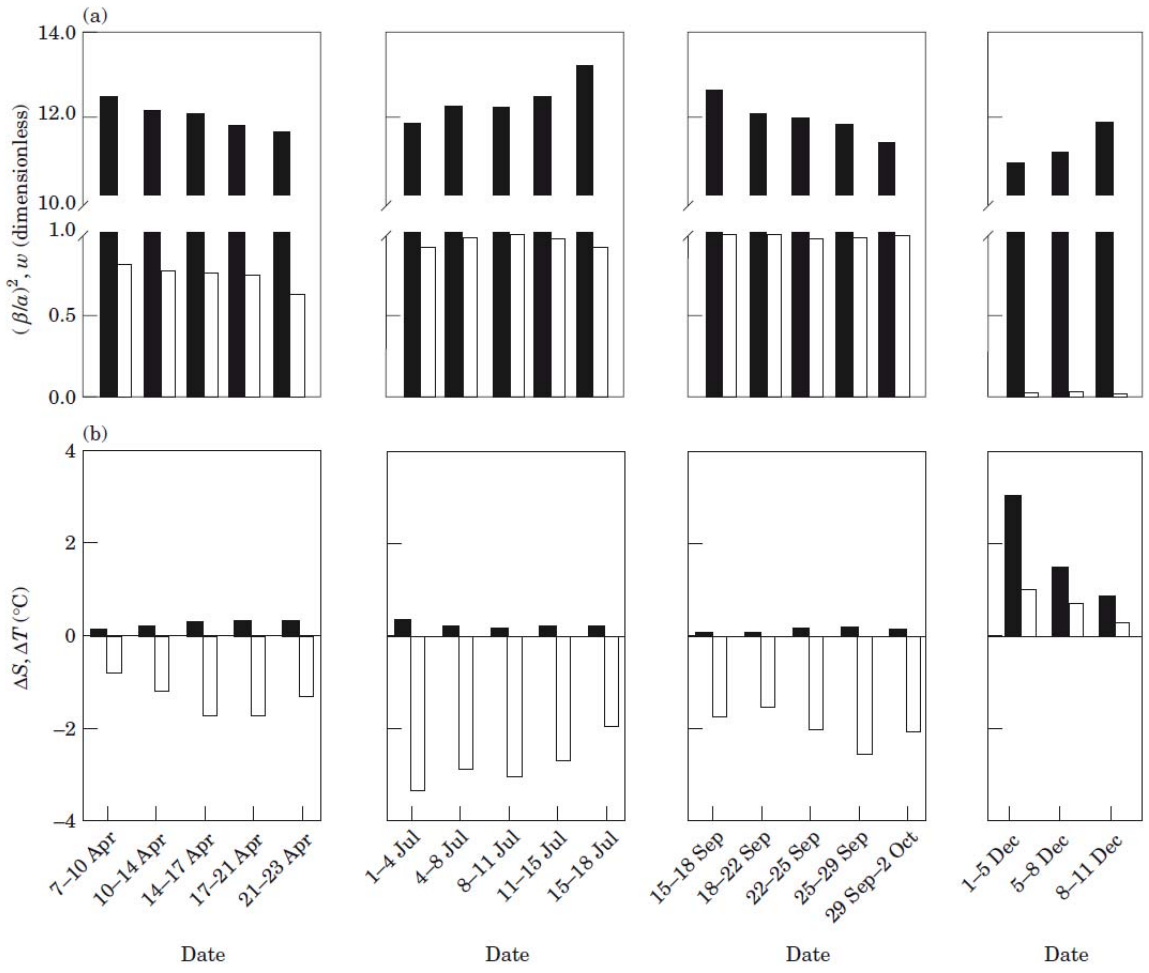

Figure 2

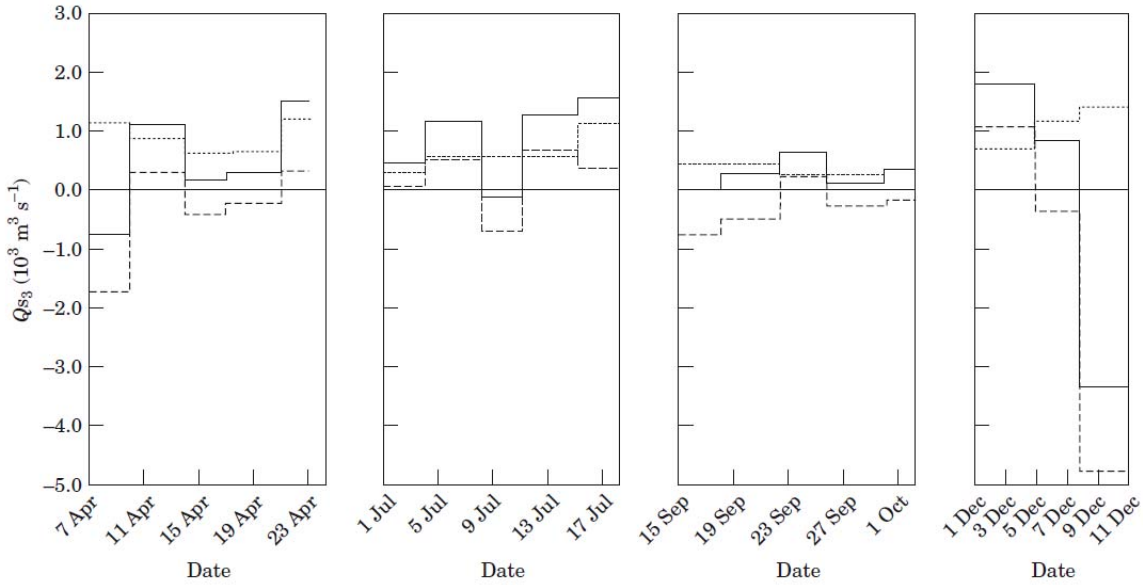

Figure 3

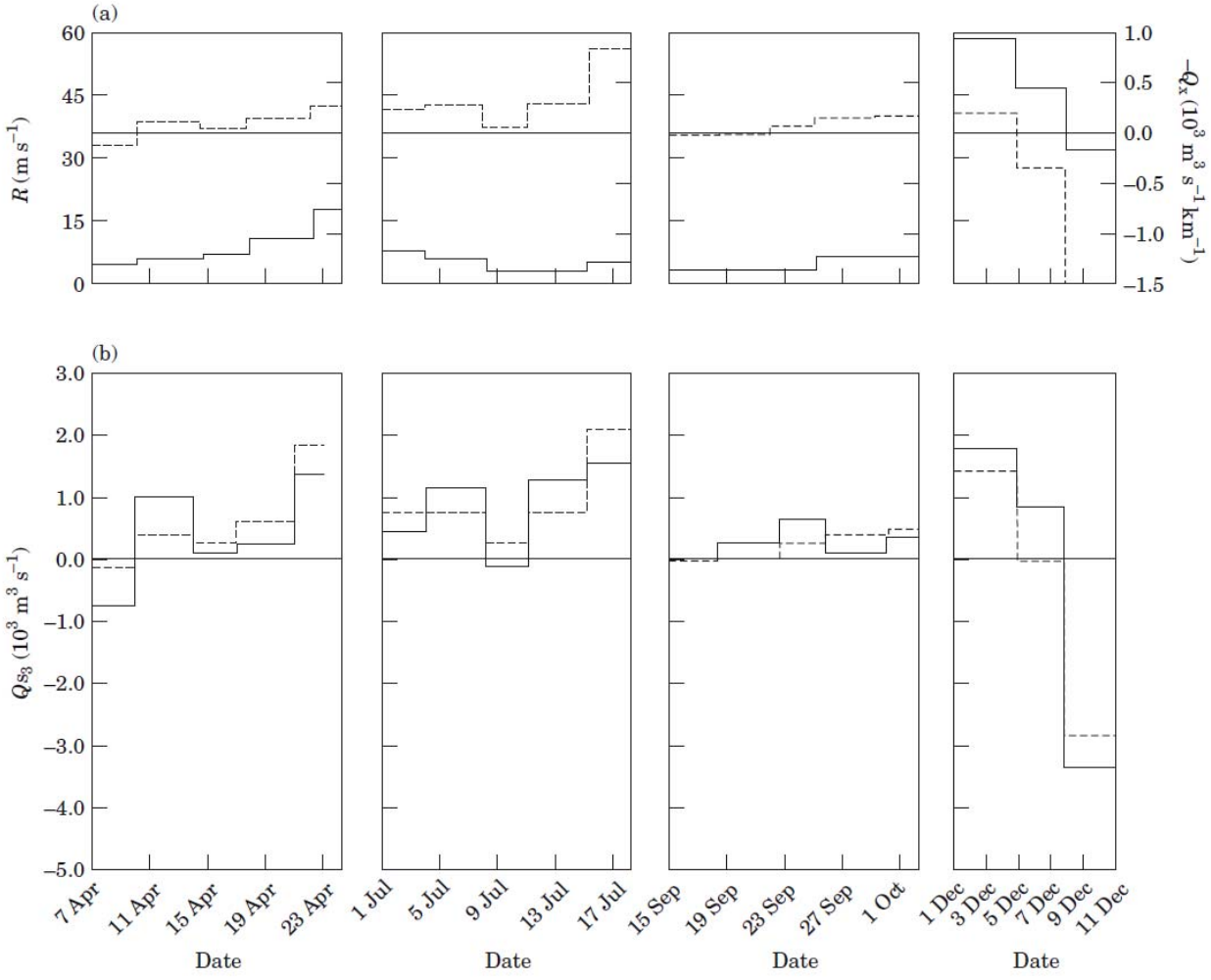

Figure 4

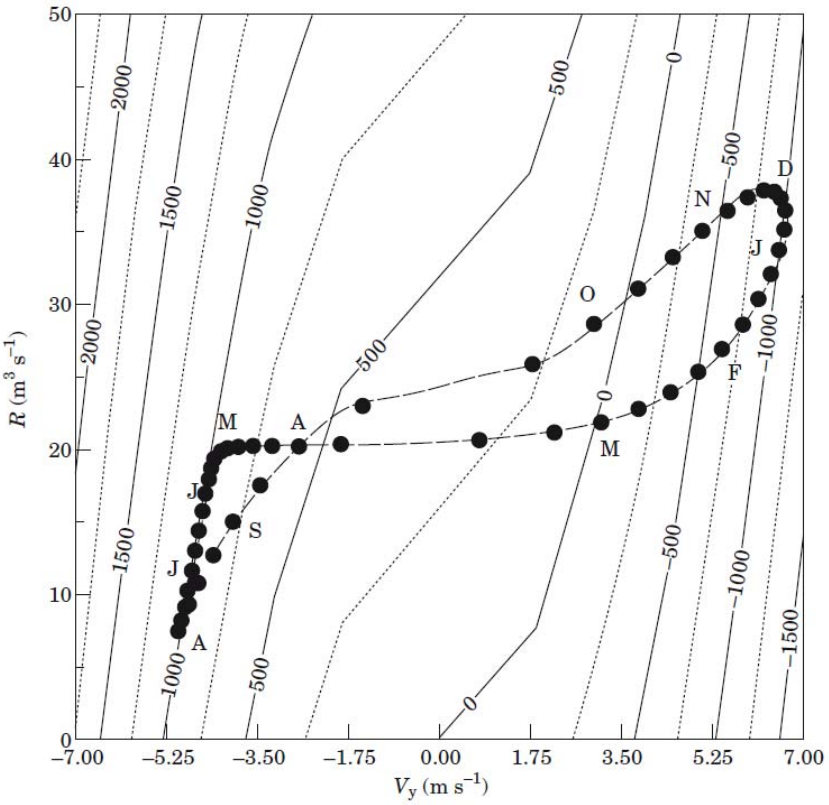

Figure 5

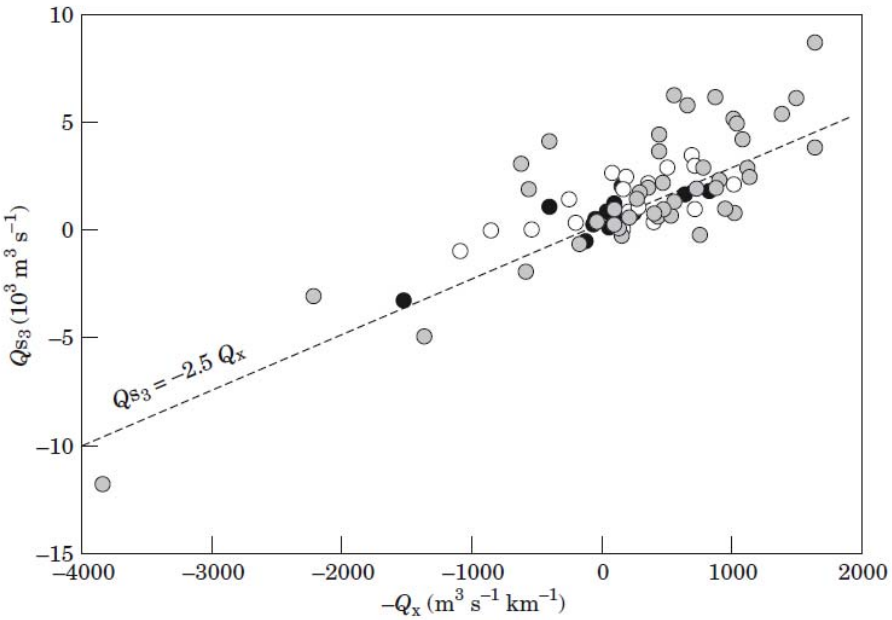

Figure 6

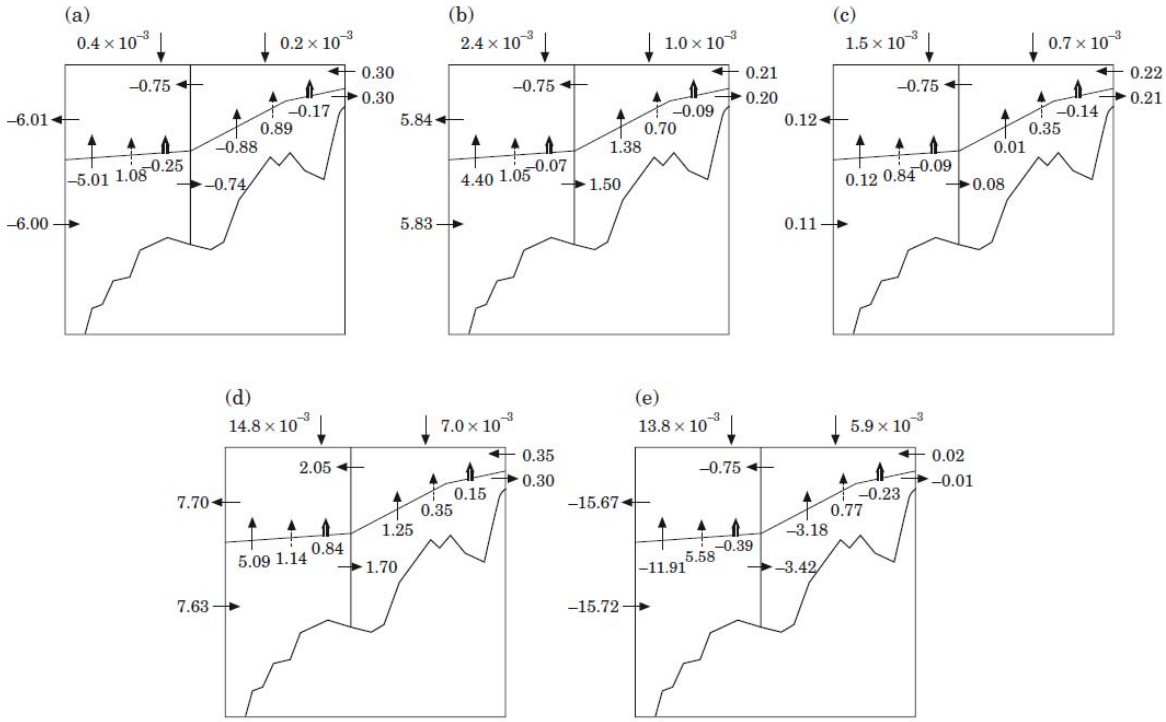
(a)
0.4 × 10−3
0.2 × 10−3
−0.75
0.30
0.30
−6.01
−0.17
0.89
−0.88
−5.01
1.08
−0.25
−0.74
−6.00
(b)
2.4 × 10−3
1.0 × 10−3
−0.75
0.21
0.20
5.84
−0.09
0.70
1.38
4.40
1.05
−0.07
1.50
5.83
(c)
1.5 × 10−3
0.7 × 10−3
−0.75
0.22
0.21
0.12
−0.14
0.35
0.01
0.12
0.84
−0.09
0.08
0.11
(d)
14.8 × 10−3
7.0 × 10−3
2.05
0.35
0.30
7.70
0.15
0.35
1.25
5.09
1.14
0.84
1.70
7.63
(e)
13.8 × 10−3
5.9 × 10−3
−0.75
0.02
−0.01
−15.67
−0.23
0.77
−3.18
−11.91
5.58
−0.39
−3.42
−15.72

Figure 7